protocols.io

Quantitative Magnetization Transfer MR Imaging (qMT-MRI) of Diabetic Mouse Kidney V.2 🔗

Feng Wang[1], Takamune Takahashi[1]

[1]Vanderbilt University

Oct 16, 2019

| 1 | *Works for me* | dx.doi.org/10.17504/protocols.io.8a7hshn

Lili Liang ⚡

ABSTRACT

Summary:

This protocol describes the procedures and data acquisition of quantitative magnetization MR imaging of diabetic mouse kidney.

Reference:

1. Zhao, H.J., et al., *Endothelial nitric oxide synthase deficiency produces accelerated nephropathy in diabetic mice.* J Am Soc Nephrol, 2006. 17(10): p. 2664-2669.

2. Ramani, A., et al., *Precise estimate of fundamental in-vivo MT parameters in human brain in clinically feasible times.* Magnetic resonance imaging, 2002. 20(10): p. 721-31.

3. Cercignani, M. and G.J. Barker, *A comparison between equations describing in vivo MT: the effects of noise and sequence parameters.* Journal of Magnetic Resonance, 2008. 191(2): p. 171-83.

4. Pluim, J.P.W., J.B.A. Maintz, and M.A. Viergever, *Mutual-information-based registration of medical images: A survey.* Ieee Transactions on Medical Imaging, 2003. 22(8): p. 986- 1004.

5. Wang, F., et al., *Repeatability and sensitivity of high resolution blood volume mapping in mouse kidney disease.* J Magn Reson Imaging, 2014. 39(4): p. 866-71.

6. Smith, S.A., et al., *Measurement of T1 and T2 in the cervical spinal cord at 3 tesla.* Magnetic resonance in medicine : official journal of the Society of Magnetic Resonance in Medicine / Society of Magnetic Resonance in Medicine, 2008. 60(1): p. 213-9.

7. Henkelman, R.M., et al., *Quantitative Interpretation of Magnetization-Transfer.* Magnetic Resonance in Medicine, 1993. 29(6): p. 759-766.

Diabetic Complication:

Nephropathy

EXTERNAL LINK

https://www.diacomp.org/shared/document.aspx?id=303&docType=Protocol

NAME ⌄	CATALOG # ⌄	VENDOR ⌄
C57BLKS	C57BLKS	Jackson Laboratory

MATERIALS TEXT

Animals: The DN mice (db/db eNOS-/-, 15-24 weeks, 38-60 g) were prepared as described previously [1]. The WT mice (wild type, 9 weeks, 20-28 g) with C57BLKS background were purchased from the Jackson Laboratory (Bar Harbor, ME). All animal procedures were approved by the Institutional Animal Care and Use Committee (IACUC) at Vanderbilt University.

Note:

Jackson Laboratory (RRID:SCR_004633)

1   **MRI:** All MR images were acquired on a 7T horizontal bore imaging system. A Doty 38-mm inner diameter transceiver coil was used due to the large size of the diabetic mice. Anesthesia was induced and maintained with a 1.5%/98.5% isoflurane/oxygen mixture, and a constant body temperature of 37.5ºC was maintained using heated air flow. The structural imaging protocols used a field-of-view (FOV) of 34x34 mm2 . For kidney segmentation, water images (Fig. 1a-c) were obtained based on 3-point Dixon reconstruction (gradient echo sequence, TR =45 ms, flip angle = 35º, and multiple TEs were around 4, 4.5 and 5ms).

To ensure that the same region was sampled for quantitative measures in non-invasive MRI and histological sections, quantitative magnetization transfer (qMT) data were collected separately for left and right kidneys at the equatorial position for each kidney. This orientation of kidney is much easier to be defined than other orientations in histologic section. One example of the placement of a single oblique coronal slice at the equatorial position of the kidney was shown in Figure 1. We used both axial and sagittal anatomical images (Fig. 1a&b) to place the equatorial coronal slice (Fig. 1c). The qMT data set was collected using a 2D MT-weighted spoiled gradient recalled-echo sequence (TR 24 ms, flip angle =7º, matrix size 256x256, 24 acquisitions, resoltuion = ~0.133x0.133x1 mm3). Gaussian-shaped saturation pulses (θsat = 220º and 820º, pulse width = 10 ms) were used. The first data set was collected with 12 different RF offsets and a constant logrithmic interval ranged between 1 and 80 kHz for general quality of regional MT spectra in kidney (Fig. 1d). Previous qMT imaging of human brain has suggested the minimal number of RF sample points [2, 3]. However, due to the motion artifacts in kidney imaging, we acquired 7 RF offsets ranged between 1 and 80 kHz at two saturation powers to ensure an accurate modeling and derivation of qMT parameters in this study (which required ~34 min of imaging time). Observed relaxation rate R_{1obs} were obtained based on images acquired with two flip angles. B_1 map was based on images acquired with two flip angles, whereas B0 map was based on two gradient echo images (ΔTE = 2 ms).
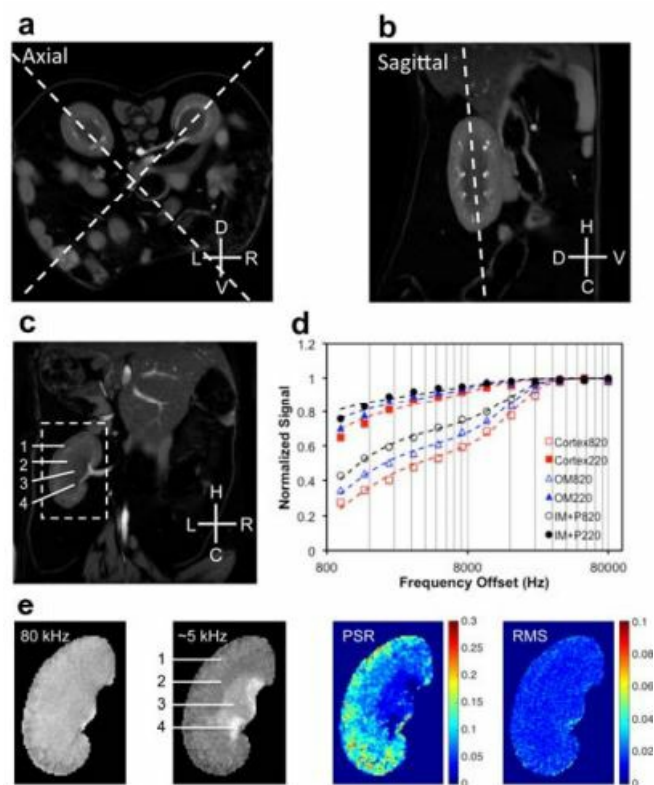
Figure 1. qMT data acquisition and quantification. (a-b) Examples showing the selection of equatorial coronal orientation for qMT data acquisition. This equatorial orientation is better for further comparison between MRI and histological results. Dashed lines indicate the selected equatorial orientations on axial or sagittal images for qMT data acquisition. L: left; R: right; D: dorsal; V: ventral; H: head; C: caudal. The axial and sagittal images are the water images from 3-point Dixon construction, and these images highlight kidneys in diabetic mice (DN mouse shown). (c) The water equatorial coronal image from 3-point Dixon reconstruction. 1-cortex, 2-outer medulla (OM), 3-inter medulla and papilla (IM+P), 4-extra renal space. (d) The example fitting of the model to regional MT data in kidney at two flip angles of θ_{sat} 220° and θ_{sat} 820°. (e) Segmented qMT images zoomed on the left kidney at RF offsets at 80 and ~5 kHz, pool size ratio (PSR) map with color-coded values, and root mean squares of the residuals (RMS) from model fitting.

2 **Data Analysis:** All MRI data were analyzed using MATLAB 2014b (The Mathworks). All intrasession images used in quantification were coregistered using a rigid registration algorithm based on mutual information [4]. Kidneys were manually segmented based on T_1-weighted images (Fig. 1c) [5]. T_{1obs} was obtained using the dual-angle approach [6].

Figure 1d compares the representative normalized signals obtained from voxels in cortex, outer medulla (OM), and inner medulla and papilla (IM+P) of kidney at different MT saturation powers (θ_{sat} = 220° and 820°) and frequency offsets. Henkelman-Ramani's model was applied to derive qMT parameters [2, 3].

$$SI(\omega_1, \Delta f) = \frac{M_0\left(R_b[\frac{RM_{0b}}{R_a}] + R_{RFB}(\omega_{1CWPE}, \Delta f, T_{2b}) + R_b + \frac{RM_{0b}}{F}\right)}{[\frac{RM_{0b}}{R_a}](R_b + R_{RFB}(\omega_{1CWPE}, \Delta f, T_{2b})) + (1 + \left[\frac{\omega_{1CWPE}}{2\pi\Delta f}\right]^2[\frac{1}{T_{2a}R_a}])(R_{RFB}(\omega_{1CWPE}, \Delta f, T_{2b}) + R_b + \frac{RM_{0b}}{F})} \quad (1)$$

where **a** and **b** denote the free water pool and macromolecular pool, respectively. F is the relative size of the macromolecular pool, defined as F=M_{0b}/M_{0a}. M_{0a} and M_{0b} are the fully relaxed values of magnetization associated with the two pools, and M_0 is the signal without MT-weighting.

The continuous wave power approximation (CWPE) was applied and ω_{1CWPE} is the amplitude of the saturating field [2, 3]. Δf represents the frequency offset of the MT pulse. R_{RFB} is the rate of saturation of longitudinal magnetization in pool b due to the irradiation by the amplitude defined by ω_{1CWPE} and Δf [3], which is also dependent on the transverse relaxation time of the macromolecular pool T_{2b}. A super-Lorentzian line shape is used to represent the bound pool [3]. T_{2a} is the transverse time of free water pool. R is the exchange rate constant. Ra and Rb are the respective longitudinal relaxation rates. Additional constraints were imposed to determine qMT parameters. R_b was kept fixed at 1 s⁻¹ as usual [2, 3, 7]. Another constraint was imposed by measuring the observed longitudinal relaxation rate R_{1obs} independently, which was linked to Ra [7].

$$R_a = R_{1obs} - RM_{0b}(R_b - R_{1obs})/(R_b - R_{1obs} + \frac{RM_{0b}}{F}) \quad (2)$$

M_0, F, RM_{0b}, T_{2a} and T_{2b} were determined from the model fitting. The PSR was defined as the "F" value from the fitting. The fitting quality at each pixel was evaluated by the root mean squares (RMS) of the residuals at each RF offset. The corresponding PSR and RMS maps and selected images with MT contrast (MTC) were shown in Fig. 1e.

T_1-weighted and MTC images were used for manual selection of ROIs (regions of interests) such as cortex, OM, IM+P, and extra-renal space for quantification (Fig. 1c&e). The regions with fibrosis were selected according to their high PSR values. The normal PSR range was defined as Mean ± 2SD (standard deviation, 95%) of the normal WT mice, and regions with significantly higher PSR was defined as voxels with PSR out of this normal range. Regions with PSR higher than different threshold at Mean+2SD, Mean+3SD, or Mean+4SD were detected and percent areas of those regions in the cortex were calculated. The positive threshold PSR (tPSR) was quantified as

$$tPSR = \frac{Area\ (PSR > threshold)}{Total\ Area} \times 100\% \quad (3)$$

The significance of measurement differences was evaluated using Student's t-tests. The correlations between tPSR and histological results were further calculated across kidneys, using the Pearson correlation function.